

Sizing It Up: Cellular MRI Using Micron-Sized Iron Oxide Particles

Erik M. Shapiro,* Stanko Skrtic, and Alan P. Koretsky

There is rapidly increasing interest in the use of MRI to track cell migration in intact animals. Currently, cell labeling is usually accomplished by endocytosis of nanometer-sized, dextran-coated iron oxide particles. The limitations of using nanometer-sized particles, however, are that millions of particles are required to achieve sufficient contrast, the label can be diluted beyond observability by cell division, and the label is biodegradable. These problems make it difficult to label cells other than macrophages *in vivo*, and to conduct long-term engraftment studies. It was recently demonstrated that micron-sized iron oxide particles (MPIOs) can be taken up by a number of cell types. In this study we examined the MRI properties of single MPIOs with sizes of 0.96, 1.63, 2.79, 4.50, and 5.80 μm . Furthermore, the capacity of cells to endocytose these MPIOs was investigated, and the MRI properties of the labeled cells at 7.0 and 11.7 Tesla were measured as a function of image resolution and echo time (TE). Cells labeled with MPIOs generally contained iron levels of ~ 100 pg, which is approximately threefold higher than those obtained with the best strategies to label cells using nanometer-sized particles. On occasion, some cells had levels as high as ~ 400 pg. We demonstrate that these large particles and the cells labeled with them can be detected by spin echo (SE)-based imaging methods. These measurements indicate that MPIOs should be useful for improving cell tracking by MRI. *Magn Reson Med* 53:329–338, 2005. Published 2005 Wiley-Liss, Inc.†

Key words: MRI; iron oxide; cells; contrast agents; particles

Cellular imaging with MRI has proven useful for many applications, including noninvasive monitoring of stem cell migration and homing (1–3), t-cell trafficking (4), and macrophage infiltration (5). Most often, cells are loaded with dextran-coated iron oxide nanoparticles (USPIO, MION) (6), but iron oxide-based dendrimers have also proven to be effective labeling agents (7). When there is sufficient iron oxide labeling, it is possible to detect single cells *in vitro* (8), and a few cells *in vivo* (9), creating the exciting possibility that the migration of single cells in an animal can be detected.

There are a number of limitations in MRI cell tracking. The first is that millions of nanometer-sized particles are necessary to achieve detection. This requires highly efficient labeling schemes for robust detection (10). The need to get a large number of nanoparticles into cells for MRI has limited MRI-based cell tracking to requiring that most cells be labeled *in vitro* and then reintroduced into the

animal. The only exception has been macrophages, which avidly take up injected dextran-coated iron oxide nanoparticles *in vivo* (11).

Two other issues with MRI-based cell tracking that can limit its applicability are that cell division can dilute the label beyond detectability, and the dextran-coated particles are biodegradable. After several weeks, the particles are broken down and the iron is recycled by the cell, which can cause loss of detection and toxicity (12,13). These disadvantages can hamper any study in which long-term engraftment and stability are being examined or very slow migration is anticipated.

We recently reported that cells can be labeled with polymer-encapsulated 0.96- μm -sized iron oxide particles (MPIOs) (14). These particles have higher relaxivity than USPIOs, based on equivalent iron content, by nearly 50% (14) and are readily available. We further demonstrated that a single MPIO can be reliably detected in single cells and 11.5-day-old mouse embryos (15). The ability to detect cells labeled with single particles may have a number of advantages over labeling cells with millions of nanometer-sized dextran-coated particles. Their polymer coating should be inert to the cell, allowing long-term studies of labeled cells and their progeny. Since cell division can only dilute particles down to single particles, at least some of the daughter cells can be followed after each cell division. Finally, the need to label cells with only one particle may open up possibilities for labeling cells *in vivo*.

In our previous works, 0.96- μm MPIOs were used (14,15). However, larger particles are now available and offer the possibility of greatly increasing iron content. In this study, we investigated the capacity of cells to endocytose particles of five different sizes (diameter = 0.96, 1.63, 2.79, 4.50, and 5.8 μm), and performed MRI at 7.0 and 11.7 Tesla with different imaging resolutions and echo times (TEs). Additionally, we quantified the MRI properties of single particles in agarose gels. Lastly, we explored the possibility of using T_2 -based contrast methods to visualize individual particles and labeled cells, as opposed to the more commonly used method of using susceptibility-based T_2^* measurements.

MATERIALS AND METHODS

Murine hepatocytes were isolated from female C57Bl/6 mice by the collagenase perfusion method followed by repeated centrifugations, according to Seglen (16). Isolated hepatocytes were suspended and cultured in DMEM/F-12 medium (GIBCO, Gaithersburg, MD) with 5% fetal bovine serum, 2 mM glutamine, 0.875 μM bovine insulin, 100 nM dexamethasone, 5 ng/ml EGF, 100 U/ml penicillin, and 100 $\mu\text{g}/\text{ml}$ streptomycin. Cells were plated at a density of 1×10^6 cells/cm² on plastic culture flasks (TissueCulture;

Laboratory of Functional and Molecular Imaging, National Institute of Neurological Disorders and Stroke, National Institutes of Health, Bethesda, Maryland.

*Correspondence to: Erik M. Shapiro, National Institute for Neurological Disorders and Stroke, National Institutes of Health, Bethesda, MD 20892. E-mail: ShapiroE@ninds.nih.gov

Received 24 June 2004; revised 30 August 2004; accepted 30 August 2004.
DOI 10.1002/mrm.20342

Published online in Wiley InterScience (www.interscience.wiley.com).

Published 2005 Wiley-Liss, Inc. † This article is a US Government work and, as such, is in the public domain in the United States of America.

Greiner, Longwood, FL) and allowed to attach. Murine embryonic fibroblasts were grown according to instructions from the supplier (ATCC, Gaithersburg, MD) and plated at 1×10^6 cells/cm². The porcine mesenchymal stem cells were a gift from Dr. Venkatesh Raman (NHLBI, NIH). The neuronal precursor cells were a gift from Dr. Jose Antonio Rodriguez (NINDS, NIH). For cell labeling with MPIOs, 10–100 μ l of 3×10^8 encapsulated superparamagnetic microspheres were added to the growth medium, and incubated with the cells for 18 hr. The diameters of the particles (Bangs Laboratories, Fishers, IN) were 0.96, 1.63, 2.79, 4.50, and 5.80 μ m. The Bangs particles consisted of a magnetite core coated with a divinyl benzene/styrene polymer. COOH functionality was introduced to the surface of the particles. A fluorescent dye was soaked into the polymer coating of some of the particles. The 4.50- μ m particles were obtained from Dynal Biotech (Oslo, Norway). Dynal particles consist of a magnetite core coated with a polystyrene polymer. Control cells were incubated without particles.

To remove free particles after labeling, the cells were first washed extensively to remove loosely bound free particles. The cells were then released from the dish by incubation with trypsin. To remove additional free MPIOs, the cells were pelleted and resuspended in growth medium at 10^6 /ml, and density centrifugation was performed with Ficoll-Paque PLUS (Amersham Biosciences, Piscataway, NJ). Briefly, 3 ml of Ficoll-Paque PLUS was added to 15-ml plastic Falcon tubes. Then, 3 ml of resuspended cells were layered on top of the Ficoll-Paque PLUS, with care taken to not disturb the interface. The tubes were centrifuged for 30 min at $400 \times g$. After centrifugation, most of the free particles had pelleted to the bottom of the tube, and the cells remained at the interface of the Ficoll-Paque PLUS and growth medium. The cells were removed with a glass pipette and washed with growth medium to remove trace Ficoll-Paque PLUS. For imaging purposes, the cells were transferred onto eight-well chamber slides (Lab-Tek II; NUNC, Rochester, NY), at 50 cells per well, and allowed to attach. Growth medium was made with 1 mM Gd-DTPA (Magnevist, Berlex) to shorten T_1 to allow rapid MRI. Trypan blue exclusion tests were performed at each step to measure cell viability. The cells labeled with the 4.50- μ m MPIOs were immersed in agarose, 1 mM Gd-DTPA, in a disposable culture tube.

We analyzed the physiology of the labeled cells by generating two point growth curves and cell division assays on the culture dish. Two point growth curves were generated for fibroblasts labeled with 1.63- and 2.79- μ m MPIOs and unlabeled fibroblasts. Following the density centrifugation step, cells were plated at three different densities in T25 cell culture flasks (10^3 , 10^4 , or 10^5 cells per flask). Three days later the cells were trypsinized and counted in triplicate. Migration and cell division assays were performed by plating 10^3 fibroblasts labeled with 1.63- and 2.79 μ m MPIOs and unlabeled cells, in separate wells of six-well culture dishes. Cells were plated in a concentrated 10-mm area in the center of the wells. Cell numbers and areas of occupancy were monitored at 1, 4, and 7 days post-plating by light and fluorescence microscopy (Leica stereo-fluorescence microscope; Leica Microsystems, Inc., Bannockburn, IL), as well as by full-field fluorescent im-

aging of the entire six-well dish with a Typhoon 9400 fluorescence plate reader (Amersham Biosciences, Piscataway, NJ). We acquired 25- μ m fluorescence images with the Typhoon plate reader using both green (for cells labeled with 1.63- μ m MPIOs) and red (for cells labeled with 2.79- μ m MPIOs) laser excitation and emission. All quantification of the images used programs written in Interactive Data Language (IDL; Research Systems Inc., Boulder, CO). Fluorescence counts were measured, and because of the extremely high image resolution of the Typhoon, each fluorescence count was assumed to be a single cell with one or more fluorescent particles inside. Additionally, cell area was measured. Comparisons with the unlabeled cells were made with images acquired on the stereo-fluorescence microscope.

T_2^* -weighted 3D gradient-echo (GRE) imaging was performed at 7.0 and 11.7 T (Bruker Biospec), with three different TEs: 3, 5, and 10 ms. Images were acquired at 200 μ m³ and 100 μ m³, and $100 \times 50 \times 50$ μ m resolution. Other imaging parameters were TR = 100 ms, and FOV = $5.12 \times 2.20 \times 0.64$ cm. T_2 -weighted 3D spin-echo (SE) imaging was performed with a rapid acquisition with relaxation enhancement (RARE) readout at 7.0 T, with three different effective TEs (22, 45, and 68 ms) at 200 μ m³ and 100 μ m³, and $100 \times 50 \times 50$ μ m resolution. Other imaging parameters were TR = 300 ms, FOV = $5.12 \times 2.20 \times 0.64$ cm, and echo train length (ETL) = 4. We used 35-mm birdcage coils tuned to the respective Larmor frequencies. The tube containing the cells labeled with 4.50- μ m MPIOs was imaged at 4.7T using similar image parameters, specifically described in the caption of Fig. 8. Fluorescent and light microscopy were used at each point to verify label and cellular integrity.

The sizes of the susceptibility induced signal decrease caused by the cells loaded with MPIOs were measured using programs written in Interactive Data Language. The 3D MRI data sets were reconstructed to best analyze the layer of cells directly on the culture dish. Images were then thresholded at the noise level, and the sizes of seven random hypointense areas were measured by counting pixels. This was done for the data from the three different echo times and at the two different field strengths. This was done for the data from the three different TEs and at the two different field strengths.

Agarose phantoms of dispersed, single MPIOs for MRI were constructed by adding 2×10^3 particles to 1% agarose in microtubes, which resulted in ~ 15 particles in each 50- μ m slice. The microtubes were sealed and then immersed in agarose doped with 100 mM MnCl₂. The agarose exterior prevents large susceptibility artifacts around the tubes, and manganese doping was used to eliminate MRI detectable signal from the outside agarose, allowing a smaller field of view (FOV). MRI was performed in a manner similar to that used for the labeled cell samples. T_2^* -weighted 3D GRE imaging was performed at 7.0 T with three different TEs: 3, 5, and 10 ms. Images were acquired at 200, 100, and 50 μ m³ resolution. Other imaging parameters were TR = 100 ms, and FOV = $2.56 \times 2.56 \times 1.28$ cm. T_2 -weighted 3D SE imaging was performed with a RARE readout at 7.0 T, with four different effective TEs: 28 (8.6 ms echo spacing); 40 (10 ms echo spacing); 60 (15 ms echo spacing); and 80 (20 ms echo

Table 1

Particle size (μm)	Iron/particle (pg)	% magnetite (w/w)	Fluorescence (ex, em)
8.50	9.40	3.80	480, 520
5.80	4.40	5.30	None
4.50	10.3	20.0	None
2.79	1.50	12.2	660, 690
1.63	1.10	42.5	480, 520
0.96	0.125	27.8	480, 520

spacing) ms at 200^3 , 100^3 , and 50^3 μm resolution. Other imaging parameters were TR = 300 ms, FOV = $2.56 \times 2.56 \times 1.28$ cm, and ETL = 8. A 35-mm birdcage coil tuned to the respective Larmor frequency was used.

To quantify the contrast from the different size particles and different imaging conditions, signal profiles were plotted through the hypointense regions for seven dark spots. The plot profiles were normalized to the average signal intensity of control tubes without particles for each imaging condition. We approximated the size of the contrast region by measuring the full width at half height of the signal hypointensity profiles. T_2^* and relaxivity calculations were made on the un-normalized data using the point of maximum signal decrease. Relaxivity, R , was calculated both on a per-particle basis and on an iron concentration basis, using the iron content per particle as reported in Table 1.

$$\frac{1}{T_2} - \frac{1}{T_2^0} = R[\text{particle}] \text{ or } R \times \left[\frac{\text{iron content per particle (mmoles)}}{\text{voxel volume (liters)}} \right]$$

RESULTS

Table 1 summarizes information about the different-sized particles. The 4.5- μm particles have the most iron per particle, followed by the 8.5- and 5.8- μm particles. Over the wide range of sizes there is an 80-fold change in iron content per particle. Additionally, while the largest particles contain the most iron by volume, it is clear that they are far from full, and a significant increase in iron content is possible. All particles are commercially available, and some are fluorescently labeled and contain iron oxide.

MRI of single particles in agarose was performed. Figure 1a shows an MR image of single MPIOs in agarose at 100- μm isotropic resolution, with a TE of 10 ms. No hypointense areas were detected in the control samples, and the size and hypointensity of particles varied among the different-sized MPIOs. Figure 1b quantifies the MRI results for the different MPIOs as 1D normalized average intensity profiles through seven dark spots in each sample. As expected, the particles with the highest iron content—the 4.50- μm MPIOs (10.3 pg iron/MPIO) and the 8.50- μm MPIOs (9.40 pg iron/MPIO)—generated the largest susceptibility-induced decrease in signal intensity using T_2^* weighting. These particles created a hypointense region ~ 200 μm large, and reduced the signal intensity by $72.1\% \pm 1.8\%$ and $67.0\% \pm 9.0\%$, respectively, of the background signal intensity. The 5.80- μm (4.40 pg iron/MPIO) generated the next-largest signal voids (again ~ 200 μm large) while reducing the signal intensity by $46.7\% \pm 4.1\%$. Smaller particles with nearly equivalent iron content—2.80- μm (1.50 pg iron/MPIO) and 1.63- μm (1.1 pg iron/MPIO)—generated signal voids similar in size. The contrast generated by these particles was $40.0\% \pm 3.4\%$

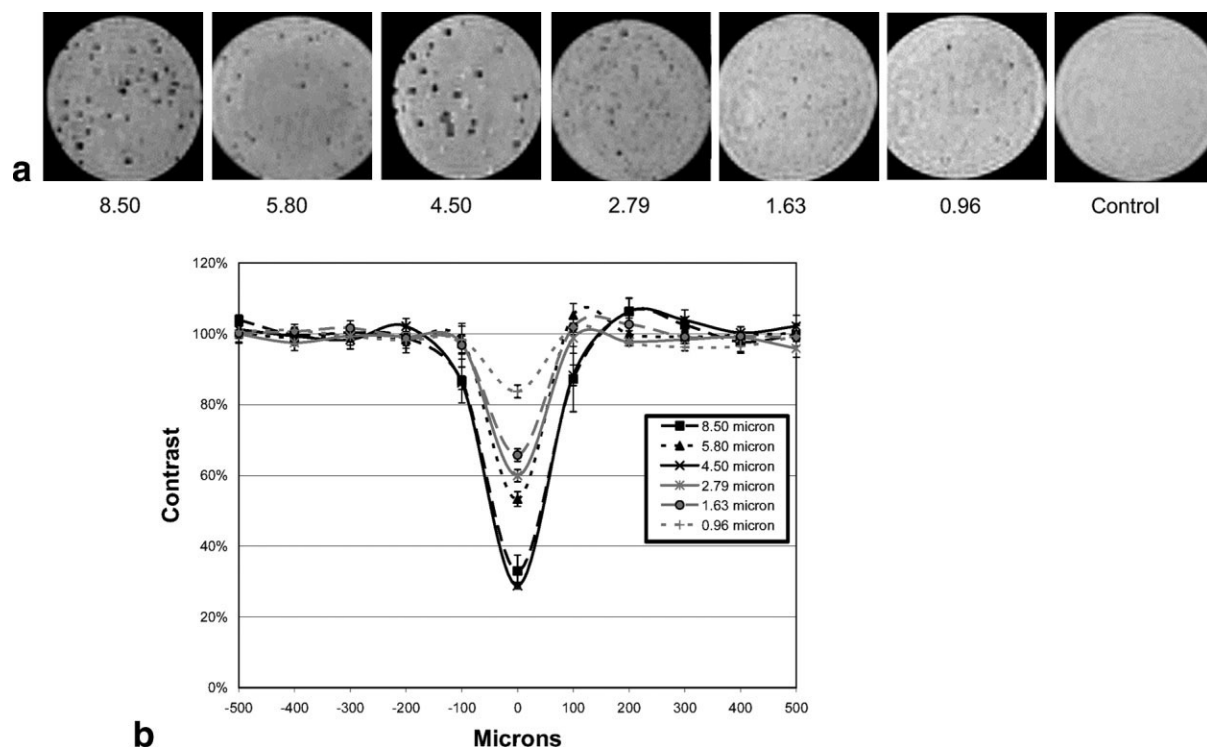


FIG. 1. T_2^* -weighted GRE-MR images of single MPIOs of various sizes. **a**: MR images of seven different samples, with different-sized MPIOs. MRI was performed at 7.0 T with a 10-ms TE, and at 100- μm isotropic resolution. **b**: Average profile plots for each size MPIO.

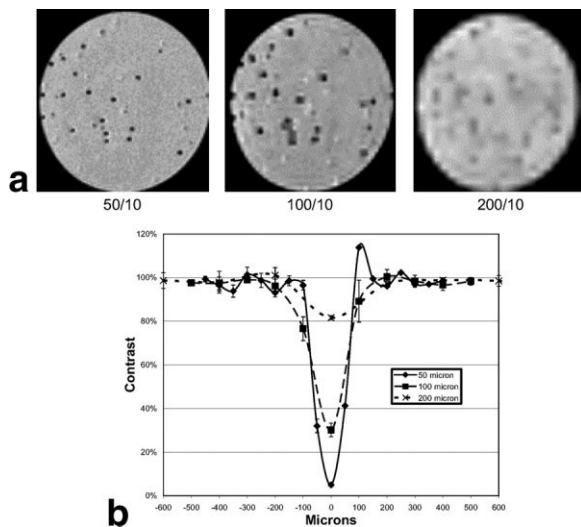


FIG. 2. Single 4.5- μm MPIO GRE-MR image. **a**: Imaging parameters are given as resolution/TE for each image. **b**: Average profile plots for three different image resolutions.

and $34.3\% \pm 3.5\%$, respectively. Lastly, particles with the lowest iron content ($0.96 \mu\text{m}$; $0.125 \text{ pg iron/MPIO}$) exhibited the smallest susceptibility-induced contrast areas, and caused a decrease in intensity of $16.3\% \pm 3.6\%$. In all cases, single particles were visible. This shows that it is possible to detect single MPIOs, as previously reported (15). Regions of hyperintensity were detected around the particles, and were most pronounced around the larger particles. The hyperintensity was aligned along the frequency-encoding direction and is presumably due to the well-known effects that a dipole field will have on resonance frequency in T_2^* -weighted MRI (17).

Figure 2 shows that the susceptibility-induced hypointensity depended on the pixel size. Figure 2a shows images of the tube containing the 4.50- μm particles, at 10-ms TE using three different image resolutions. These are all from the same area of the tube, for proper registration of particles. Figure 2b shows that the depth of the hypoin-

tensity increased as the pixel size decreased from 200 μm to 50 μm . There was a $95.0\% \pm 3.5\%$ decrease in signal intensity for the 50- μm image, compared to a $69.8\% \pm 6.2\%$ decrease for the 100- μm image and a $18.4\% \pm 6.4\%$ decrease for the 200- μm image. The smaller degree of hypointensity caused by the particles of the lower-resolution images is due to partial volume effects. The bandwidth was changed for each resolution to maximize the signal-to-noise ratio (SNR), with the two higher-resolution experiments having larger readout bandwidths. Therefore, the percent decrease in signal intensity does not directly coincide with the ratio of voxel sizes. Rather, the hypointensity of the lower-resolution images is larger than it would have been had the larger bandwidths used in the higher-resolution images been maintained for the lower-resolution images.

Figure 3 shows the effects of increasing TE on MRI of the particles. The hypointense regions due to the particles increased with longer TE (Fig. 3a). Figure 3b and c show average plot profiles for two particle sizes: 4.50- and the 1.63- μm , respectively. Comparing the two particle sizes, the 4.50- μm particles generated more contrast than the smaller, 1.63- μm particle. Based on the signal profiles, apparent T_2^* values were calculated, for the particles as well as for the agarose from a region without any particles, and the results were used to calculate relaxivities of single particles at 100- μm resolution. Using the point of the maximal signal decrease, the T_2^* values were 6.6 ms for a pixel with a single 4.50- μm particle, and 16.1 ms for a 1.63- μm particle. The background T_2^* was 48.1 ms. Using these values, the apparent relaxivity for the 4.50- μm particle at 100- μm isotropic resolution is $130.7 \text{ s}^{-1}\text{particle}^{-1}$, while the relaxivity of the 1.63- μm particle at 100- μm isotropic resolution is $41.32 \text{ s}^{-1}\text{particle}^{-1}$. Thus the 4.50- μm particle has a threefold higher relaxivity. Interestingly, the apparent relaxivities on a per-iron basis are $2286 \text{ s}^{-1}\text{mM}^{-1}$ for the 4.50- μm particles, and $6759 \text{ s}^{-1}\text{mM}^{-1}$ for the 1.63- μm particles. This may reflect the different properties of the iron oxide crystals themselves, including domain size, the proximities of the domains to each other, and included impurities.

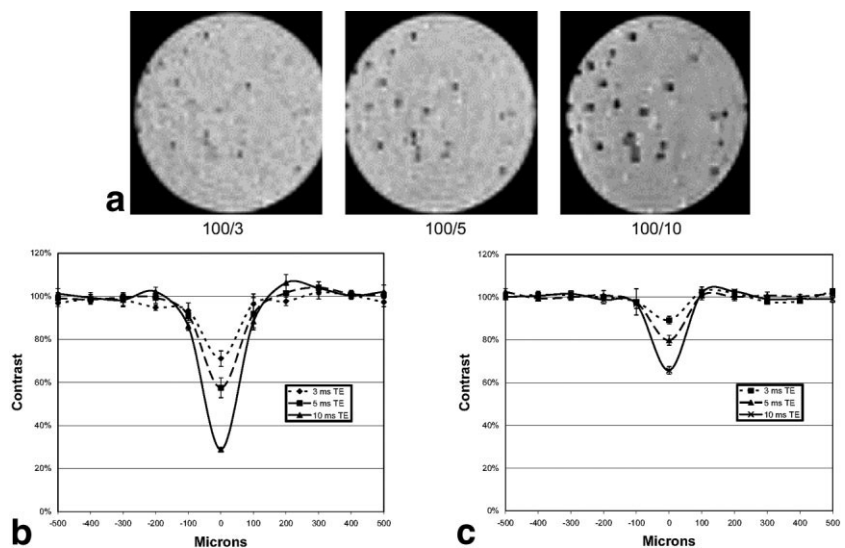


FIG. 3. Single 4.5- μm MPIO GRE-MR image. **a**: Imaging parameters are given as resolution/TE for each image. Average plot profiles at 100- μm resolution, for three different TEs for (b) 4.50- μm MPIO, and (c) 1.63- μm MPIO.

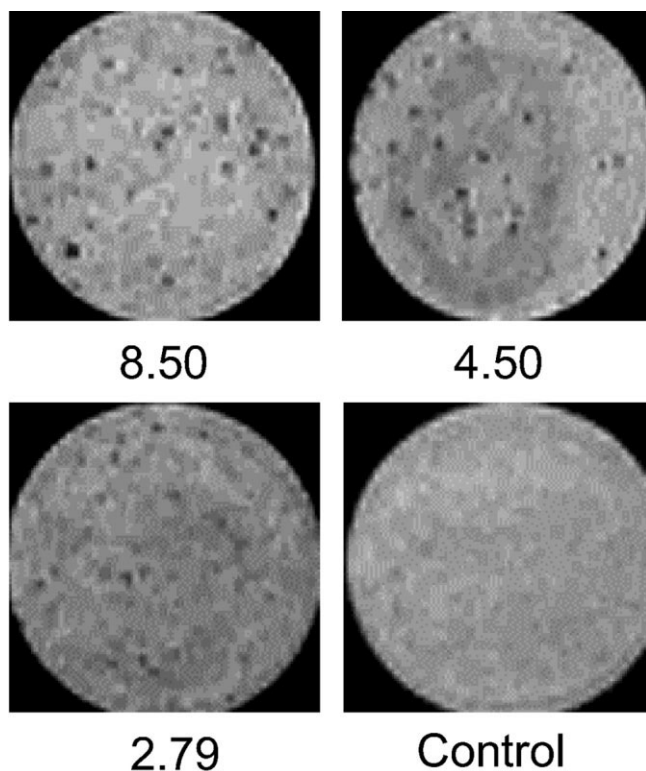


FIG. 4. Single-particle 3D SE-MRI at 100- μm isotropic resolution, 60-ms effective TE, with an 8-ETL RARE readout. Particle sizes are indicated below images.

T_2 -weighted, SE MRI using a RARE readout was performed as well. The results are shown in Fig. 4. Echo spacings of 10–20 ms at pixel resolutions of 100- μm were

used. Hypointensity in the T_2 -weighted MR image was readily detected for the 8.5- and 4.5- μm MPIOs. Smaller signal changes were detected for the 2.79- μm MPIO, and no significant hypointensities were detected for the smaller particles (data not shown). Additionally, these hypointensities became more robust with longer echo spacings. Hypointense contrast was small at 200- μm resolution, even for the largest particles.

To determine whether mammalian cells would take up the larger particles in culture, we labeled the murine primary hepatocytes with the five different-sized MPIOs. Figure 5 shows light microscopy images of five hepatocytes (one each for the different-sized MPIOs) attached to a second cell culture dish. Clusters of dark, perinuclear spheres can be seen in each hepatocyte. One can also see that the particles are in close proximity to each other, and are not randomly scattered throughout the cell. Labeling efficiency was $\sim 90\%$ for all MPIO sizes. Cell death as measured by the trypan blue exclusion method was 5% for all but the 4.50- μm MPIOs, which caused approximately 10% cell death.

It is clear from Fig. 5 that the 4.5- and 5.8- μm MPIOs can be readily observed with just light microscopy. To verify that the dark regions were due to particles for the smaller MPIOs, fluorescence images were compared with light microscopy images. Figure 6 shows a hepatocyte labeled with 2.79- μm MPIOs. There is excellent correspondence between the dark area in light microscopy (Fig. 6a) and the fluorescence detected for the particle (Fig. 6b). Using both light and fluorescence microscopy, we counted the numbers of particles per cell. For instance, we counted 38 particles in the cell shown in Fig. 6, which is a typical number. Counting the smaller particles revealed ~ 100 for the 1.63- μm MPIOs and ~ 300 for the 0.96- μm MPIOs per cell. Using the data in Table 1, we estimated the cellular

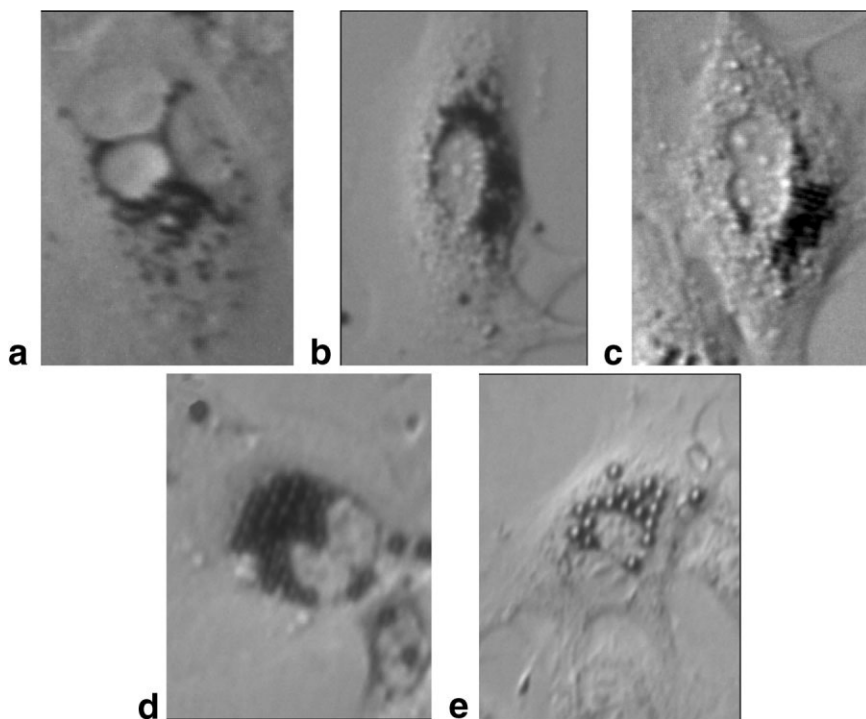


FIG. 5. Light microscopy images of hepatocytes labeled with (a) 0.96-, (b) 1.63-, (c) 2.79-, (d) 4.50-, and (e) 5.80- μm particles. Dark perinuclear spheres are individual MPIOs. Particle numbers per cell ranged from several hundred for the smaller particles to tens for the largest particles. **d** and **e**: Thirty-five 4.5- μm and 17 5.8- μm particles, yielding iron contents of ~ 387 and 75 μg iron, respectively.

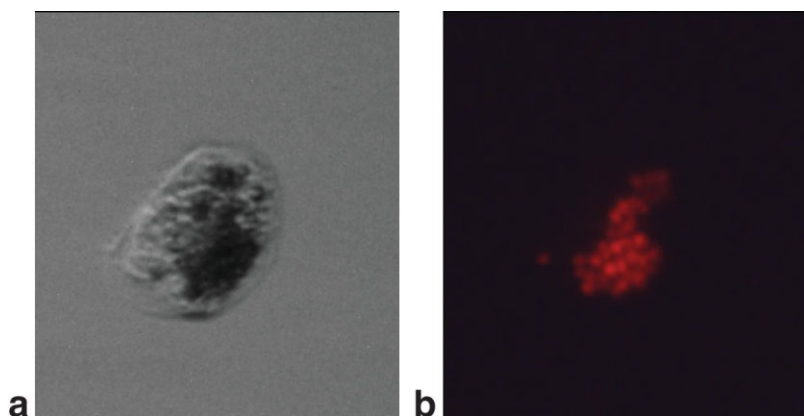


FIG. 6. (a) Bright-field and (b) red fluorescent image of a hepatocyte labeled with 2.79- μm MPIOs. The cell is in suspension, following washing.

iron contents. The results were 75–100 pg for the 5.80-, 4.50-, 2.79-, and 1.63- μm MPIOs, and \sim 37.5 pg iron for the 0.96- μm MPIO-labeled cells.

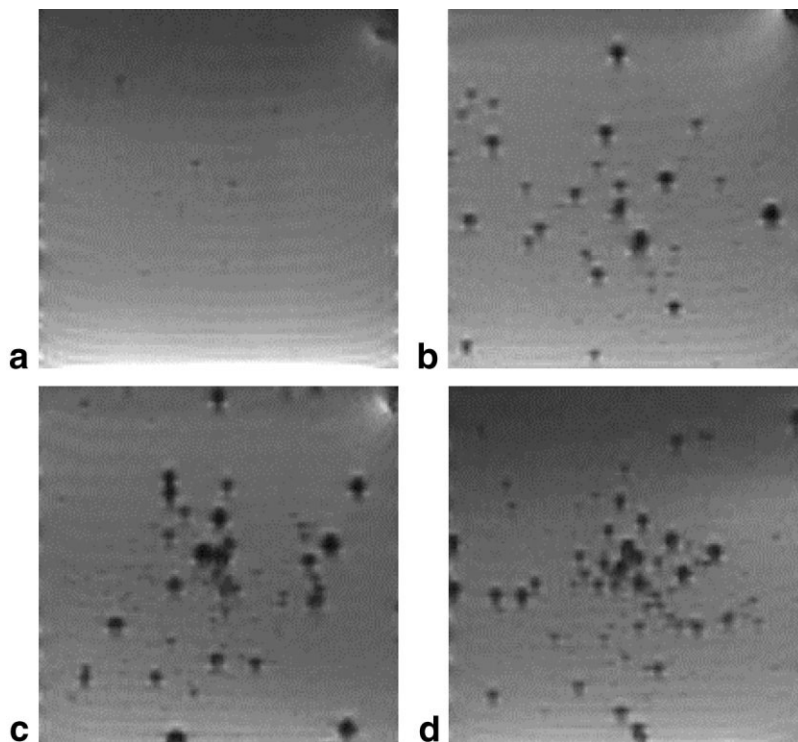
Figure 7 shows representative MR images of cells labeled with the three smallest MPIOs and unlabeled cells. These images were acquired at 7.0T at 100- μm isotropic resolution with a TE of 10 ms. Readily visible are numerous, “arrowhead”-shaped dark signal areas surrounded by bright halos. In this case, the main magnetic field is aligned from the bottom of the figure to the top. This is the signal shape that a superparamagnetic sphere should create with Fourier imaging, when the slice plane is transverse to the main magnetic field (17). These dark signal areas differ slightly in size, most likely because of differential labeling between cells.

Since the 4.50- μm MPIOs produced the most robust signal voids as single particles, we labeled the hepatocytes with these particles and imaged them with both GRE and

SE imaging techniques. For this experiment, hepatocytes were suspended in agarose. Figure 8a shows one slice from a 3D GRE data set at 100- μm isotropic resolution with a 10-ms TE. Two different-sized contrast regions can be seen in this image: smaller signal voids (presumably from free particles that had not been separated from the cells, or cells with one or few particles) and larger signal voids from well-labeled cells. Figure 8b shows the same slice from a 3D-SE RARE data set, with 100- μm isotropic resolution and 40 ms effective TE (10 ms echo spacing, 8 ETL). Large signal voids can still be observed, even with T_2 weighting, registering exactly with the largest signal voids from the GRE image. The contrast from the free particles nearly goes away.

The areas of the dark susceptibility contrast regions were measured as a function of MPIO size, field strength, and GRE time, using the slices containing the cells at the bottom of the chamber slide. Figure 9 summarizes these

FIG. 7. (a) Unlabeled and (b) 0.96- μm -, (c) 1.63- μm -, and (d) 2.79- μm -labeled hepatocytes. Images were acquired at 7.0 T at 100- μm isotropic resolution, with a TE of 10 ms.



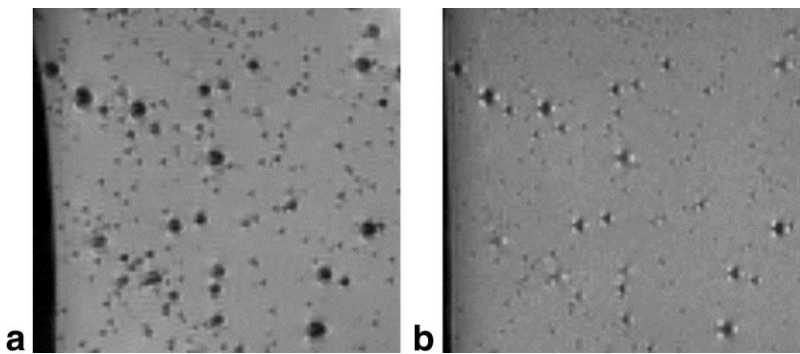


FIG. 8. 100- μm isotropic MR image of 4.5- μm MPIO-labeled hepatocytes using (a) GRE, 10-ms TE; and (b) SE RARE, 40-ms effective TE, 10-ms echo spacing, and ETL = 8.

three variables two different ways: on a per-cell basis, and on per-MPIO basis. Figure 9a demonstrates that the size of the signal voids, across all samples and field strengths, were not statistically different for different-sized MPIOs, for matching TEs. In fact, the average areas of the contrast regions from the 100- μm isotropic resolution images, across all samples at 10 ms TE, was 13.21 pixels with a standard deviation (SD) of 1.26 pixels. For the images acquired at 5 ms, the average area was 8.10 ± 0.93 pixels. At 3-ms TE, the average area of the contrast regions was 5.35 ± 0.82 pixels. The second observation is that lengthening the TE increased the area of the signal voids, as expected for susceptibility-induced contrast. Lengthening the TE from 3 to 5 ms increased the areas of the contrast regions by $152\% \pm 13\%$, while lengthening the TE to 10 ms increased the contrast area by $249\% \pm 30\%$. Signal voids measured from the $100 \times 50 \times 50 \mu\text{m}$ resolution images were equivalent to those measured from the 100- μm isotropic resolution images. The 200- μm isotropic resolution images had severe susceptibility artifacts at the base of the chamber slide, which precluded accurate signal void measurements. Data on a per-MPIO basis provides additional insights. Figure 9b graphs the data vs. the particle number. The numbers of particles per cell were 35, 100, and 300 for cells labeled with the 2.79-, 1.63-, and 0.96- μm MPIOs, respectively. These are the average numbers of particles per cell, as described above. Here it is established that particles with more iron content are more efficient at causing hypointensity than MPIOs with less iron, an analogous result to the single particles in agarose data. Interestingly, the number of particles that were taken up led to similar amounts of total iron per cell.

Finally, several different cell types were labeled with various-sized MPIOs. Figure 10 shows two light microscopy images detailing the extent of labeling for two cell types. Figure 10a shows a field of rat neuronal progenitors labeled with 5.80- μm particles. About 50% of the cells have one or more particles incorporated inside them, with a few free particles on the dish as well. Trypan blue analysis of the cells directly on the dish revealed $>95\%$ viability after labeling. Figure 10b shows a wide-field view of porcine mesenchymal stem cells labeled with 1.63- μm particles. Cell labeling was near 100% for these cells with the smaller particles, with $\sim 50\%$ labeling for the larger particles ($\geq 4.5 \mu\text{m}$). In addition, robust labeling of mouse embryonic fibroblasts was achieved (100% labeling, cell viability $>95\%$, data not shown). Growth curves for fibroblasts labeled with 1.63- and 2.79- μm MPIOs were not

significantly different from each other or the unlabeled cells for the three plating concentrations. Additionally, cell division assays using large-FOV bright-field and fluorescence imaging showed that areas of extent of migration of dividing labeled cells were not different from each other or unlabeled cells. In fact, the number of cells with one or more green fluorescent 1.63- μm MPIOs increased 1.7 times over the first 4 days, and 2.6 times over the entire 7 days. The areas the cells occupied increased 1.7 times and 3.6 times over the same time points. Most importantly, cells on the outer edges of the cell growth area, which were cells that only arose through cell division, contained one or more fluorescent particles.

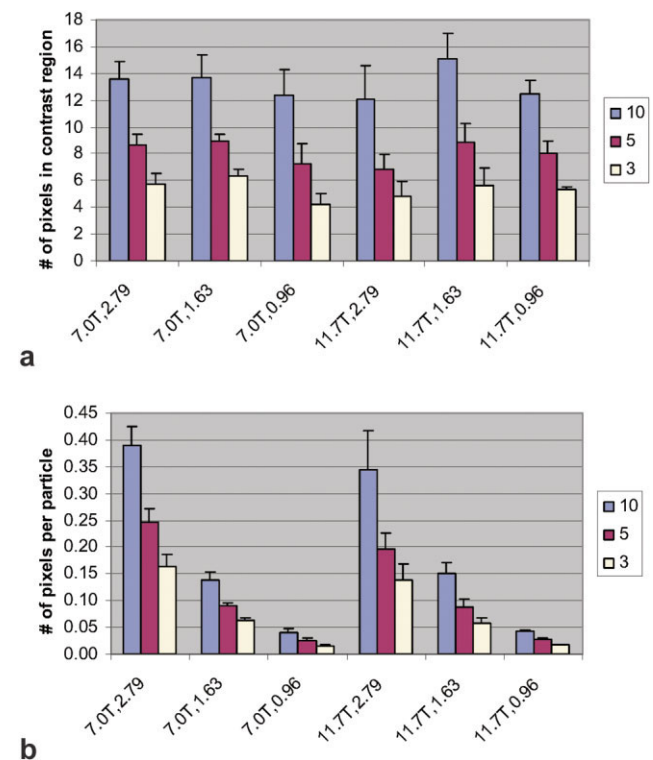


FIG. 9. Graphic representation of the measured areas of the contrast regions created by cells labeled with the three different MPIOs, at the two field strengths, different GRE times, and 100- μm isotropic resolution. **a:** Per-cell basis. **b:** Per-particle basis. The X-axis labels indicate field strength and MPIO, and the data labels reflect the TE used in the experiment. Error bars are +SD.

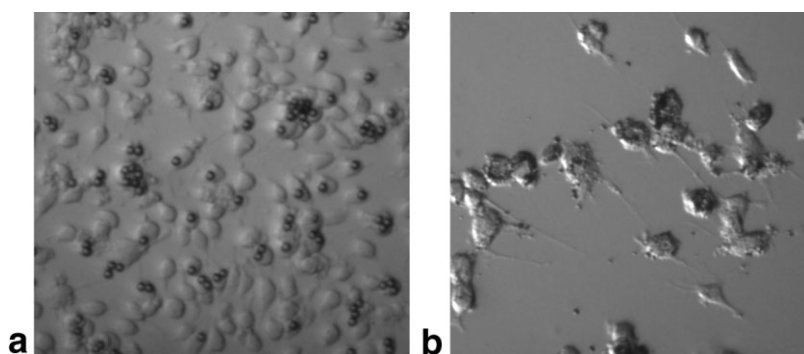


FIG. 10. Wide-field light microscopy images of (a) rat neuronal precursors labeled with 5.80- μm particles, and (b) porcine mesenchymal stem cells labeled with 1.63- μm MPIOs.

DISCUSSION

We have demonstrated the usefulness of MPIOs for efficiently labeling cells with superparamagnetic iron oxide. Cells readily endocytose MPIOs from 0.96 μm in diameter to as large as 5.80 μm without the aid of lipofection agents (18) or modification of the surface (19), as is often done with dextran-coated iron oxide nanoparticles. Labeling can be accomplished simply by incubating adherent cells with the particles for a time suitable for good labeling efficiency (normally 12–18 hr for labeling of >75% of cells). Iron contents near 100 pg were routinely achieved with most sizes of particles, with loading as high as 387 pg iron observed (Fig. 5d). Furthermore, viability, as assessed by trypan blue exclusion assays, indicated that the cells remained alive after labeling. Further evidence that the cells tolerated the particles is that only live cells reattached to a second culture vessel following trypsinization, as shown in Figs. 5 and 10.

We previously showed that the differentiated function and proliferative capacity of mesenchymal and hematopoietic stem cells were not affected by labeling with 0.96- μm MPIOs (14). We also showed that cell morphology and alkaline phosphatase expression were similar in labeled and unlabeled cells. In this study we observed that many particles were concentrated in one or more endosomes. Since particles do not spontaneously cluster in suspension, because of their surface charge, this suggests active packaging by live cells. Furthermore, the increase in the number of cells containing fluorescent particles indicates that particles were distributing in daughter cells following cell division. It will be interesting to test cell function in a variety of cells labeled with the larger MPIOs in future work.

Evidence that cells can tolerate these particles comes from our earlier work in which we injected particles into single-cell embryos that went on to develop normally (15). Single-cell mouse embryos were injected with 50–100 1.63- μm MPIOs and then allowed to develop for 11.5 days. The injected embryos looked identical in form and size to the non-injected embryos (15). This study demonstrated no difference in growth curves for labeled and unlabeled cells, or in the cells' capacity to divide and expand their population. The preliminary results with two model systems, MPIO-labeled hepatocyte transplantation and MPIO-labeled neural stem cell migration, indicate that cells labeled by MPIOs exhibit normal physiology (20). Because cell viability and activity may be linked with labeling content, more studies are necessary to determine whether

labeled cells perform specific functions. Future studies will include apoptosis assays, similar to those previously performed (14,18), as a function of particle and labeling content.

Toxicity due to iron release is a major concern with the use of iron oxide particles. A well-labeled cell with 15 pg of iron in the form of dextran-coated iron oxide nanoparticles presents a cellular concentration of ~ 250 mM iron! Cell death due to iron overload can occur at concentrations above 1 mM (21,22). Since dextran-coated particles can be degraded by the microenvironment of the lysosome, there is a danger that excessive loading of cells with dextran-coated particles may induce cell death due to iron overload. Most studies to date have not detected significant toxicity, but this remains a major concern. Particles coated with an inert matrix, such as the MPIOs described here, potentially can prevent this.

This study provides a framework for magnetic cell labeling with MPIOs, which can be tailored to a specific purpose. Three cases are particularly relevant. The first case is one in which a cell is labeled *in vitro* and delivered *in vivo*, and is not expected to undergo a large number of cell divisions. Here it may not be important which size MPIO is used for cell labeling, because the important issue is how much iron the cell takes up. The graph in Fig. 8a shows that the signal void caused by a labeled cell is largely independent of particle size when it is well labeled. It is interesting that similar amounts of total iron were achieved independently of particle size. It is likely the case that particles are trapped in endosomes/lysosomes, and cells have a fixed capacity for the volume of these compartments. However, there still may be ways to optimize the labeling procedure to maximize the number of large particles.

The second case is when cells are labeled *in vitro* and transplanted *in vivo*, and a large number of cell divisions are expected, as in the case of a stem cell. Since cell division will dilute the label, to maintain detection of the maximum number of daughter cells, one would want to use particles where the highest number of particles can be endocytosed, while being able to preserve robust single particle detection. In this case, the particles with higher iron content (>0.96 μm) would be preferred. Last is the case of direct *in vivo* labeling. Here, labeling efficiency is expected to be low due to delivery and accessibility. In this case, one would want to use only the particles with the highest iron content. In this way, even if a single

particle is endocytosed, robust detection of the labeled cell will still be possible. Preliminary results indicate that neuronal precursor cells within the subventricular zone of rodents can be labeled *in vivo* with MPIOs (20).

Single cells have been robustly visualized *in vitro* (8), and the detection of small clusters of a few cells *in vivo* has been claimed (9). As yet, there have been no reports of the detection of single labeled cells *in vivo*. This challenge stems largely from low iron labeling of cells, too many background “dark spots,” and a too-low imaging resolution. Measuring the areas of the signal voids at different TEs can be used as a starting point for designing experiments aimed at single-cell detection *in vivo*. In an MR experiment, the maximal TE that can be used depends greatly on the background susceptibility of the tissue. Two examples of high-field imaging in rodents are the brain, where a long T_2^* allows TEs as long as 10 ms, and bone marrow, where the short T_2^* prohibits TEs much longer than 3 ms. The average signal void area from a well-labeled cell at 10 ms TE was ~ 13 pixels at 100- μm isotropic resolution. At that resolution, this corresponds roughly to an area 3 pixels by 4 pixels, which should be easily and reliably detectable in rodents. If the pixel size had to be increased to 200 μm , the signal void area would decrease to 3–4 pixels total, which is still detectable. Lower resolution than that, however, would put a strain on the robustness of the detection. At 3-ms TE, the average area of the dark contrast regions was ~ 5.5 pixels. At 100- μm resolution, this represents an area of roughly 3 pixels by 2 pixels; again, this should be easily detectable. However, imaging at 200- μm isotropic resolution would result in a contrast area of 1 or 2 pixels total, which is still detectable but difficult. This analysis suggests that the minimum resolution one should aim for in attempting to visualize single cells depends on the tissue involved. The data indicate that in the rodent brain, a resolution of 200- μm isotropic or better should be sufficient to detect MPIO-labeled cells, but in bone marrow, liver, or other tissues with short T_2^* , 100- μm isotropic or better may be required. Of course, these conditions may change if and when particles with much higher iron content become available or other breakthroughs in loading efficiency are achieved. This would allow the use of even shorter TEs to achieve the same degree of visualization, which in turn would decrease the number of nonspecific hypointensity regions caused by phenomena other than iron particles, such as blood vessels or air–tissue interfaces.

This work justifies further research into the development of novel particles larger than 1 μm . The particles used in this study all had a relatively low percentage of iron. For example, the 2.79- μm particles had an iron content of only 12.2%, or 1.5 pg per particle. If this iron loading could be increased to 90%, yielding ~ 10 pg iron per particle, then the 75 pg of iron the cells currently can be loaded with could be increased to 500 pg without increasing the number of endocytosed particles! Fully maximizing the capacity of these larger particles with efficient iron loading would dramatically increase the susceptibility of such a particle, and hence its potency, making single-particle detection inside single cells more robust even at lower, clinically relevant image resolutions. Labeling cells with these particles might alleviate the

stress of efficient labeling schemes, and perhaps permit *in vivo* labeling of cell populations. Continued work to determine the upper size limit for particle endocytosis by several cell types is under way, with an emphasis on improving labeling efficiency for the MPIOs described herein.

Lastly, most cellular MRI studies use GRE experiments to take advantage of the susceptibility difference labeled cells create in the tissue. However, GRE-MRI suffers from the problems of image distortion and artifacts with extended TEs. In addition, tissues have shorter T_2^* than T_2 . Detection of iron oxide-labeled cells with T_2 -based imaging can potentially enhance the detectability of cells by ameliorating these two effects. Furthermore, with the use of RARE readouts, images can potentially be acquired more rapidly than with standard GRE techniques. As illustrated by Fig. 8, the use of MPIOs to label cells may make it possible to use T_2 -based MRI to detect cells *in vivo*.

CONCLUSIONS

Cells can be labeled with micron-sized, polymer-encapsulated, superparamagnetic iron oxide particles, with iron loading as high as several hundred pg per cell. Particles as large as 5.80 μm were taken up effectively by the cells. The MR signals for a variety of imaging conditions were quantified, for both single particles of various sizes and labeled cells. The information obtained should be useful for determining optimal imaging parameters for single-cell detection *in vivo*. Further research into maximizing the iron capacity of large iron oxide particles, and determining the upper size and shape limits of particles for endocytosis in different cells is justified.

REFERENCES

- Bulte JW, Zhang S, van Gelderen P, Herynek V, Jordan EK, Duncan ID, Frank JA. Neurotransplantation of magnetically labeled oligodendrocyte progenitors: magnetic resonance tracking of cell migration and myelination. *Proc Natl Acad Sci USA* 1999;96:15256–15261.
- Hoehn M, Kustermann E, Blunk J, Wiedermann D, Trapp T, Wecker S, Focking M, Arnold H, Hescheler J, Fleischmann BK, Schwinott W, Buhle C. Monitoring of implanted stem cell migration *in vivo*: a highly resolved *in vivo* magnetic resonance imaging investigation of experimental stroke in rat. *Proc Natl Acad Sci USA* 2002;99:16267–16272.
- Hill JM, Dick AJ, Raman VK, Thompson RB, Yu ZX, Hinds KA, Pessanha BS, Guttman MA, Varney TR, Martin BJ, Dunbar CE, McVeigh ER, Leferman RJ. Serial cardiac magnetic resonance imaging of injected mesenchymal stem cells. *Circulation* 2003;108:1009–1014.
- Yeh TC, Zhang W, Ildstad ST, Ho C. *In vivo* dynamic MRI tracking of rat T-cells labeled with superparamagnetic iron-oxide particles. *Magn Reson Med* 1995;33:200–208.
- Dardzinski BJ, Schmithorst VJ, Holland SK, Boivin GP, Imagawa T, Watanabe S, Lewis JM, Hirsch R. MR imaging of murine arthritis using ultrasmall superparamagnetic iron oxide particles. *Magn Reson Imaging* 2001;19:1209–1216.
- Weissleder R, Elizondo G, Wittenberg J, Rabito CA, Bengel HH, Josephson L. Ultrasmall superparamagnetic iron oxide: characterization of a new class of contrast agents for MR imaging. *Radiology* 1990;175:489–493.
- Bulte JW, Douglas T, Witwer B, Zhang SC, Strable E, Lewis BK, Zywickie H, Miller B, van Gelderen P, Moskowitz BM, Duncan ID, Frank JA. Magnetodendrimers allow endosomal magnetic labeling and *in vivo* tracking of stem cells. *Nat Biotechnol* 2001;19:1141–1147.
- Dodd SJ, Williams M, Suhan JP, Williams DS, Koretsky AP, Ho C. Detection of single mammalian cells by high-resolution magnetic resonance imaging. *Biophys J* 1999;76(1 Pt 1):103–109.

9. Kircher MF, Allport JR, Graves EE, Love V, Josephson L, Lichtman AH, Weissleder RL. In vivo high resolution three-dimensional imaging of antigen-specific cytotoxic T-lymphocyte trafficking to tumors. *Cancer Res* 2003;63:6838–6846.
10. Kalish H, Arbab AS, Miller BR, Lewis BK, Zywicke HA, Bulte JW, Bryant LH, Frank JA. Combination of transfection agents and magnetic resonance contrast agents for cellular imaging: relationship between relaxivities, electrostatic forces, and chemical composition. *Magn Reson Med* 2003;50:275–282.
11. Zhang Y, Dodd SJ, Hendrich KS, Williams M, Ho C. Magnetic resonance imaging detection of rat renal transplant rejection by monitoring macrophage infiltration. *Kidney Int* 2000;58:1300–1310.
12. Weissleder R, Stark DD, Engelstad BL, Bacon BR, Compton CC, White DL, Jacobs P, Lewis J. Superparamagnetic iron oxide: pharmacokinetics and toxicity. *AJR Am J Roentgenol* 1989;152:167–173.
13. Skotland T, Sontum PC, Oulie I. In vitro stability analyses as a model for metabolism of ferromagnetic particles (Clariscan), a contrast agent for magnetic resonance imaging. *J Pharmacol Biomed Anal* 2002;28:323–329.
14. Hinds KA, Hill JM, Shapiro EM, Laukkanen MO, Silva AC, Combs CA, Varney TR, Balaban RS, Koretsky AB, Dunbar CE. Highly efficient endosomal labeling of progenitor and stem cells with large magnetic particles allows magnetic resonance imaging of single cells. *Blood* 2003;102:867–872.
15. Shapiro EM, Skrtic S, Sharer K, Hill JM, Dunbar CE, Koretsky AP. MRI detection of single particles for cellular imaging. *Proc Natl Acad Sci USA* 2004.
16. Seglen PO. Hepatocyte suspensions and cultures as tools in experimental carcinogenesis. *J Toxicol Environ Health* 1979;5:551–560.
17. Callaghan PT. Principles of nuclear magnetic resonance microscopy. Oxford, England: Clarendon Press; 1993.
18. Frank JA, Miller BR, Arbab AS, Zywicke HA, Jordan EK, Lewis BK, Bryant LH, Butle JW. Clinically applicable labeling of mammalian and stem cells by combining superparamagnetic iron oxides and transfection agents. *Radiology* 2003;228:480–487.
19. Zhao M, Kircher MF, Josephson L, Weissleder R. Differential conjugation of tat peptide to superparamagnetic nanoparticles and its effect on cellular uptake. *Bioconjug Chem* 2002;13:840–844.
20. Shapiro EM, Skrtic S, Koretsky AP. Long term cellular MR imaging using micron sized iron oxide particles. In: Proceedings of the 12th Annual Meeting of ISMRM, Kyoto, Japan, 2004.
21. Riley MR, Boesewetter DE, Kim AM, Sirvent FP. Effects of metals Cu, Fe, Ni, V, and Zn on rat lung epithelial cells. *Toxicology* 2003;190:171–184.
22. Bishop GM, Robinson SR. Quantitative analysis of cell death and ferritin expression in response to cortical iron: implications for hypoxia-ischemia and stroke. *Brain Res* 2001;907:175–187.